A reconstruction of Apennine uplift history and the development of transverse drainages from longitudinal profile inversion.

Frank J. Pazzaglia and James A. Fisher
Department of Earth and Environmental Sciences
Lehigh University
1 West Packer Ave
Bethlehem, PA 18015
fjp3@lehigh.edu

ABSTRACT

Numerous examples of transverse drainages in the Apennines inspired early, forward-thinking models to describe how rivers established and maintained their courses as mountains were being raised beneath them. We assemble the rate of base level fall (τ-U) and associated channel χ-z data of ten transverse rivers draining the Apennine pro-wedge using a channel stream power linear inverse approach. We apply the results to evaluate competing models of transverse drainage development as well as the underlying dynamic and tectonic processes responsible for Apennine topography. The channel inversion approach employs the simplifying assumption of uniform uplift and erosion at the catchment scale, but accounts for variable rock erodibility as the first-order determinant of regional, mean channel steepness. Accordingly, local deviations in channel steepness are interpreted by the model as transient upstream-propagating waves of base level fall originating at the catchment mouth. Modeled timing, rate, and unsteadiness of these base level falls are broadly consistent with geomorphic, geologic, thermochronologic, and paleo-elevation isotopic data indicating that the Apennines emerged impulsively at ~2.5 Ma at rates ranging from ~0.2-0.3 mm/yr for the central Apennines to rates of ~0.7 mm/yr for the southern Apennines. Syn-deformation, foreland-propagating superposition dominates transverse drainage development for the northern and north-central Apennines that is underlain by an intact Adriatic slab. In contrast further south where a slab window separates the Adriatic slab from the base of the Apennine wedge, dynamic uplift prevails and the transverse drainages have developed in response to regional superposition and integration of catchments through spillover and headwater capture processes.

INTRODUCTION

Rivers commonly flow transverse to structure carving impressive gorges through the mountains of their birth, yet the tectonic and surface processes that conspire to form these impressive geomorphic features has long been a topic of spirited debate (Playfair, 1802; Davis, 1889; Johnson, 1931; Meyerhoff and Olmstead, 1936; Oberlander, 1965; Twidale, 1966; Douglass et al., 2009). Three main mechanisms have emerged to explain transverse drainage development (Douglass et al., 2009): (1) self-superposition of a consequent drainage (Meyerhoff and Olmstead, 1936; Oberlander, 1965; Mazzanti and Trevisan, 1978; **Fig. 1a**), (2) antecedence and superposition from a former soft-rock cover (Davis, 1889; Johnson, 1931; **Fig. 1b**), and (3) headward extension of channels by capture (Gilbert, 1877; Brocard et al., 2012; Prince et al., 2010) or basin overflow (Meek and Douglass, 2001; Meek, 1989; Geurts et al., 2020; **Fig. 1c**). In the context of the now widely-applied stream power model for river incision, these three mechanisms make distinct predictions for catchment-wide initiation, rate, and steadiness of base level fall expressed in horizontally transformed steady-state channel profiles *(χ)* and in channel response times *(τ)* (**Fig. 1**).

Exhibiting numerous examples of transverse rivers and steep-walled gorges carved through hard rock, the Apennines form the backbone of Italian geology and topography (**Fig. 2**, X-X' and inset photo) and have engendered important research on the development of transverse drainage (Mazzanti and Trevisan, 1978; Coltorti and Pieruccini, 2000). Eastward propagation of the Europe-Adria plate boundary over the Cenozoic has embedded paired shortening and extending deformation fronts in the Apennine orogenic wedge with both subaqueous and subaerial histories (Elter et al., 1975; Cavinato and DeCelles, 1999) that can be leveraged to test prevailing models (**Fig. 1**). For example, self-superposition atop rising anticlines in the Apennine pro-wedge may occur when the river mouth could be fixed in a soft sedimentary cover at the tip of the orogenic wedge and the underlying, uplifting ridge has a long strike length, not allowing the river to adjust its course (Mazzanti and Trevisan, 1978; **Fig. 1a**). In contrast, regional superposition of a largely extant river network that had developed on a former, low relief landscape, prior to recent (Pleistocene) impulsive uplift (**Fig. 1b**) is an alternative way to develop the transverse drainage (i.e. Coltorti and Pieruccini, 2000; Amato et al., 2003). This latter model shares concepts in common with Coastal Plain superposition of streams atop a buried peneplain (Johnson, 1931)

2

and is seemingly well-supported by the numerous, locally well-preserved low-relief, but high elevation erosion surfaces in the Apennines that are cut across variable rock type and structure. Implicit in both self-superposition and regional superposition concepts is the growing recognition that paleovalleys inherited from the Messinian-drawdown of the Mediterranean has played a role in fixing the locations of many Apennine rivers (Scarselli et al., 2007). Suggestion that the current river network provided an erosional feedback to the tectonic growth of individual structures and overall uplift of the orogenic wedge is supported by the fact that many transverse canyons are located at the structural culminations of anticlines (Alvarez, 1999; Simpson, 2004). Lastly, the impact of local structures and retreat of asymmetric divides in driving headwater captures and carving of gorges, is recognized as a contributing process to Apennine transverse stream development (Mayer et al., 2003; Buscher et al., 2017; **Fig. 1c**).

A critical test of Apennine transverse drainage development and the overall youthful, rugged appearance of the topography using sedimentologic, stratigraphic, structural, and geomorphic data (Alvarez, 1999) had the dual impact of sharing the insights of the formerly little known Mazzanti and Trevesan (1978) research as well as illustrating the breath of Walter Alvarez's knowledge in furthering our understanding of the geology and geomorphology of Italy. Alvarez's approach and conclusions are used here as a launching point to better understand the development of transverse rivers in general as well as comment on the specific processes, rates, and steadiness in the tectonic and dynamic contributions to the development of Apennine topography.

In this paper, we model the base level fall histories of ten transverse rivers draining the Apennine pro-wedge to the Po-Adriatic foreland using a stream power-based linear inversion of channel longitudinal profiles. The approach contains simplifying assumptions about the uniformity of uplift and erosion at the catchment scale, but it does account for variation in the erodibility of the rocks underlying the catchment. The goal is to generate channel response time *(τ)* and horizontally transformed steady state profile *(χ)* data sets that can evaluate competing models of transverse drainage development (**Fig. 1**) as well discriminate among the underlying dynamic and tectonic processes responsible for the emergence of the Apennine orogenic wedge and subsequent topographic development of the chain. Our analysis is consistent with the general predictions of non-uniform dynamic support of Apennine topography, but it also suggests that the

emergence of the Apennines and evolution of the transverse drainage varies along strike of the range, where it is locally influenced by tectonic processes and inherited sediment routing systems as summarized in Alvarez (1999).

100 MECHANISMS OF TRANSVERSE DRAINAGE EXPRESSED IN RIVER LONGITUDINAL PROFILES

A river's longitudinal profile, a plot of channel elevation with respect to distance from the mouth (**Fig. 1**), has long been known to express a balance among external forces including the rate of rock uplift, and internal resistance to channel erosion including rock erodibility (Mackin,
105 1937; Hack, 1973; Seeber and Gornitz, 1983; Snyder et al., 2000; Whipple, 2004; Kirby and Whipple, 2012). The now familiar stream power formulation to model channel erosion (Howard, 1994) provides an objective platform to compare and contrast models of transverse drainage development using three related criteria: (1) the response time of a river channel to a transient change in base level (τ), (2) the elevation of the horizontally-transformed steady-state channel
110 profile (χ), and (3) a reconstruction of the rate of change of base level (U) over time expressed as a $(\tau\text{-}U)$ plot.

Calculating τ, χ, and U all falls out of the shape of a long profile, which is a power law relationship between reach-length gradient (m/m) of a stream channel and drainage area (m^2), a proxy for channel discharge (Hack, 1957). The resulting plot has properties of concavity (θ),
115 defined by the negative slope of the *logS-logA* regression, and steepness (k_s), defined by the intercept where A is 1 m^2,

$$S = k_s A^{-\theta} \tag{1}$$

120 Uniform rock uplift beneath a river catchment does little to change profile concavity, which has been shown to universally be ~0.45 (Mudd et al., 2018), whereas stream steepness does scale with rock uplift and basin-wide erosion (Lave and Avouac, 2001; Snyder et al., 2000; Kirby and Whipple, 2012; Lague, 2013) when a reference concavity (θ_{ref}) is applied.

The stream power model for river erosion (E) into bedrock is described as

125

4

$$E=KA^mS^n \qquad (2),$$

where K is rock erodibility, essentially a velocity with units of $m^{0.1}$ yr^{-1} for a $\theta_{ref}= 0.45$, and where the exponents m and n describe power-law dependencies for A and S. In these and subsequent equations, catchment area is considered to be steady, an assumption that is not true for the catchments in this study, but acknowledged and accounted for in the subsequent model set-up and interpretation. Also, in our application of the stream power model, discharge is assumed to linearly scale with drainage area, but it is also straightforward to weight drainage area for discharge where orographic precipitation gradients are steep.

Combining equations (1) and (2) under steady-state base level fall (uplift, U) and erosion (E) conditions when the elevation of the channel does not change over time ($dz/dt = 0$), and solving for S gives:

$$dz/dt = U - E = 0 \qquad (3a),$$

and

$$U = KA^mS^n \qquad (3b),$$

and

$$S = (U/K)^{1/n}A^{-m/n} \qquad (3c).$$

Comparing equation (1) to (3c) it is immediately evident that θ and m/n are equivalent and

$$k_s = (U/K)^{1/n} \qquad (4).$$

Because θ and k_s co-vary, it has become common practice to apply the reference mean concavity value (θ_{ref}) for all of the streams in the watershed, resulting in a normalized k_s value (k_{sn}). The value of 0.45 is commonly chosen based on both theory and observation, but as shown below, the mean θ value for Apennine catchments can be directly determined. For the case where the channel erosion is a detachment limited quarrying and plucking process, the exponent dependency on slope (n) is ~1 (Whipple, 2004). Regression through global datasets of k_s and E indicate that n may be close to 1 when the data for many orogens are considered, even though the

limited data from the Apennines on this question suggests that n may either be > 1 (Cyr et al., 2010; Kirby and Whipple, 2012; Lague, 2013) or ~1 (Glotzbach, 2015). Our model and interpretations proceed tempered by this uncertainty in the value of the n exponent. With the simplifying assumption that $n=1$ and using $\theta_{ref}= 0.45$, the units on channel steepness (k_{sn}) are $m^{0.9}$ and equation (4) becomes

$$k_{sn} = (E/K) \tag{5}.$$

Combining equations (1) and (5) and substituting dz/dx for S, an expression for the response time (τ, yrs) of the system (Whipple and Tucker, 1999) emerges:

$$(dz/dx) = ((dz/dt)/K)A^{-m} \tag{6a}$$

$$K(dz/dx) = (dz/dt)A^{-m} \tag{6b},$$

$$dt = dx / K\, A^m \tag{6c},$$

$$\tau = \int_{x_0}^{x} \frac{dx}{K|x'|A|x'|^{m}} \tag{6d},$$

where x_o is the starting distance at the mouth of the stream. Equation (6d) describes the amount of time (τ) it takes for a transient erosional step (a knickpoint) to move up the long profile as a kinematic wave (Howard, 1994; Whipple and Tucker, 1999).

Similarly, the steady state elevation of the channel can be predicted by calculating the elevation integral of the long profile, called χ (Perron and Royden, 2013), that emerges out equation (3c), where S is expressed as dz/dx. This results in a first-order, linear, separable differential equation that is integrated to result in:

$$z(x) = z(x_b) + (E/K)^{1/n} \chi \tag{7a},$$

where

$$\chi = \int_{x_0}^{x} A|x'|^{-m/n} dx' \tag{7b}.$$

In order to result in a transformed river long profile with units of length for both z and χ, a reference drainage area (A_0), typically 1 m^2, is used:

$$\chi = \int_{x_0}^{x} \left(\frac{A_0}{A(x')} \right)^{-m/n} dx'$$

(7c).

The slope of a χ-z plot, where z is elevation in meters, is k_{sn}. In this way, mean stream steepness can be measured as a function of channel distance or elevation, or in the case of non-uniform rock erodibility, for any part of the channel.   However, this method is problematic when considering changes in boundary conditions at discrete spatial domains within a catchment. This

complication arises because χ is integrated in the upstream direction, making its value dependent on of all of the downstream points. We implement a linear inverse solution of χ to find the least-squares k_{sn} value for each rock type that best reproduces fluvial topography (Gallen, 2018). Again, with the assumption that n=1, the combination of equations (5), (7a), (7b), and (7c) leads to that prediction of the steady-state elevation profile:

$$z(x) = z(x_b) + \int_{x_b}^{x} k_{sn}(x') A(x')^{-m/n} dx'$$

(8),

where z_b is the base level elevation, in meters, at the mouth of the stream.

The χ-transformed long profile (eq. 7c), the response time (eq. 6d), and the steady-state elevation (eq. 8) all provide a basis for a linear inversion of all channels in a catchment to

reconstruct a history of rate of base level fall *(U)*. This reconstruction carries the caveat that the base level fall occurs at a single point at the mouth of the stream, and the uplift of the catchment is uniform, or nearly uniform (Goren et al., 2014), an assumption that we take to be mostly true for Adriatic flank Apennine rivers given the sharp topographic contact between the uplift range and subsiding foreland at the plate boundary (**Fig. 2**). An advantage of assuming uniform uplift is

that the base level fall (uplift) history can consider non-uniform rock erodibility (Gallen, 2018), an almost certainty given the diverse geology of Apennine catchments. Although not considered in this study, it is possible to employ an inverse modeling approach that allows for non-uniform uplift assuming that rock erodibility is uniform (Pritchard et al., 2009), or that uplift follows a set function like a flexural response (Goren et al., 2014). Uniform rock type would be particularly

difficult to reconcile in the Apennines but given the regional coverage of our data, uniform uplift at the scale of a given catchment is a reasonable assumption.

Fully informed by the theoretical basis for τ, χ, and U, we now turn attention to how these long profile based predictions can discriminate among the various models of transverse drainage development, applied specifically to the Apennines (**Fig. 1**). The Mazzanti and Trevisan (1978; **Fig. 1a**) mechanism involves progressive lengthening of the river mouth and growth of the lower catchment, balanced by normal faulting at the catchment headwaters. The isostatic response to crustal shortening and subsequent lengthening of the stream mouth will result in a relative base level fall, expressed in steep channels in the lower portion of the catchment, that will be modeled as steady uplift once the catchment rises above sea level and the orogenic wedge grows self-similarly (**Fig. 1a**, solid line in the τ-U plot). The corresponding χ-z plot should be segmented, with an older, low-slope linear segment representing slow U during the period of topographic emergence, followed by a steeper but linear segment representing steady U as the wedge grows in an isostatically-compensated self-similar manner. The expected loss of headwater channels because of normal faulting may lead to tributary channels in χ-z space to plot below the main trend and contribute to an accelerated steepening (convexity) of the χ-z plot. If that is the case, the τ-U plot should show an increase in U towards the present (**Fig 1a**, dashed line in the τ-U plot). However, recent exploration of the impact of headwater drainage loss in a basin that is otherwise maintaining steady drainage area, as depicted in the **Fig. 1a** scenario, has been shown to have minimal impact on the slope of χ-z plot (Forte and Whipple, 2018) leading us to assert that we expect to see steady U for the **Fig. 1a** scenario.

Our consideration of regional superposition of antecedant drainage is predicated on the assumption that a drainage network developed on a low-relief landscape experiencing slow U, followed by a rapid, but transient pulse in U. If that transient is driven by dynamic mantle processes, it would also be expected to follow an acceleration, followed by decay. Such a transient U function would result in a diagnostic humped τ-U plot (**Fig. 1b**, solid line in the τ-U plot) and an S-shaped χ-z plot. Alternatively, the dynamic forcing is still in an early stage of growth, not yet reaching its peak. In that case, the subsequent uplift history will increase towards the present (**Fig. 1b**, dashed line in the τ-U plot) and the χ-z plot will be convex (Fig 1b, dashed line in the χ-z plot). In either scenario, there is no significant loss or gain of drainage area to potentially influence model reconstruction of the uplift forcing.

Lastly, both piracy and spillover mechanisms drive base level fall by impulsive addition of drainage area, causing a trunk channel to rapidly incise as it lowers its transport gradient. That impulsive incision event will be represented by a spike, followed by decaying U in the τ-U plot (**Fig. 1c**, solid line in the τ-U plot). The corresponding χ-z plot will have a high-elevation, low-slope segment followed by a concave segment (**Fig. 1c**, solid line in the χ-z plot). Multiple capture events may be represented by multiple, concave tributaries (**Fig. 1c**, dashed line in the χ-z plot) and multiple spikes, followed by decay in the τ-U plot (**Fig. 1c**, dashed line in the τ-U plot). The overall take away point from this exercise is to illustrate that the τ-U and χ-z plots are related and diagnostic of the three main ways in which transverse drainages are envisioned to develop.

GEOLOGIC AND GEOMORPHIC SETTING

The Apennines are an accretionary fold and thrust belt (Bally, et al., 1986) that initiated ~ 30 Ma along the southern flank of the Alps (Le Pichon et al., 1971). Crustal thickening in the pro-wedge has been driven by an influx of rock during the subduction of Adria beneath Europe (Picotti and Pazzaglia, 2008; Carminati and Doglioni, 2012) that has grown in the past several million years as the thicker, less attenuated crust of Adria has arrived at the plate boundary. Balanced cross-sections for the Apennines (Bally et al., 1986; Hill and Hayward, 1988) indicate ~130 to 150 km of subduction over the 30 Myr history of the wedge, which indicates relatively slow long-term rates at ~4 – 5 km/Myr (4 – 5 mm/yr), similar to the GPS geodetic rates (Devoti et al., 2008; Caporali et al., 2011; Bennett et al., 2012). Rapid rollback of Adria with respect to Europe has resulted in retreat and stretching of the upper plate, forming a wide zone of crustal extension in the retro-wedge (Royden, 1993; Carminati and Doglioni, 2012). The paired compressional and extensional components of the Apennine wedge is a defining tectonic characteristic with implications for drainage evolution and development of transverse rivers.

The Apennine wedge started to become emergent in the late Miocene or early Pliocene (Bartolini, 2003; Bartolini et al., 2003), as a west to east propagating wave (Picotti and Pazzaglia, 2008; Carminati and Doglioni, 2012) with competing tectonic, dynamic, and eustastic processes, and possible couplings to surface processes (Scarselli et al., 2007). The paired compressional and extensional deformation fronts near the trench and in the hinterland

respectively were exposed at this time, with the structural transition near the topographic culmination of the growing range (D'Agostino et al., 2001; Carminati and Doglioni, 2012). In this way, crustal thickening and subduction of the less attenuated, more buoyant part of Adria is a primary reason for the emergence of the range. However, the predicted mean elevation of much of the Apennines based on the isostatic compensation of observed crustal thickness is lower than the actual mean elevation of the range, indicating that there is a significant, regional dynamic mantle support (Faccenna et al., 2014). Evidence of variable mantle dynamic support for the range comes from seismology that shows Adria as an intact slab beneath the northern Apennines and Calabria, but torn, detached, or delaminated beneath much of the central and southern Apennines (Di Stefano et al., 2009; Pian Agostinetti et al., 2009; Benoit et al., 2011; Faccenna et al., 2014). Recent isotopic-based paleoelevation reconstructions for extensional basins astride the drainage divide argues for 1-2 km of surface uplift in the past ~3 Myrs (San Jose et al., 2020). This finding, and the base level fall (uplift) histories of Apennine rivers represent important, independent geomorphic observables to apportion isostatic (tectonic) and dynamic components of uplift (**Fig. 1**).

In general, the Apennine pro-wedge exposes a series of imbricate thrust sheets carrying Mesozoic and Cenozoic carbonate and siliciclastic rocks scraped off of the down-going Adriatic slab (**Figs. 3, 4, and 5**). In contrast, the retro-wedge is dominated by crustal extension and normal faulting. Ongoing thrust earthquakes beneath the Po Plain and Adriatic Sea (Pondrelli et al., 2006; Boccaletti et al., 2011; Lavecchia et al., 2012) and normal-fault earthquakes beneath the high Apennines (Lavecchia et al., 1994; Doglioni et al., 1999; Ghisetti and Vezzani, 2002; Chiaraluce et al., 2017) speak to concurrent shortening and extension in the wedge. However, with respect to the shortening, the northern Apennine mountain front contact with the Po foreland (**Figs. 2, 3a**), continuing into the central Apennines as the Adriatic coastline (**Figs. 2, 4a**), and then into the southern Apennines as the Bradonic trough (**Figs. 2, 5a**) presents a discrete point of base level fall. The pro-wedge between this point of base level fall to the Apennine topographic crest has a shared base level fall history (**Fig. 2**). This ~40-60 km wide zone has comparatively less seismicity and associated crustal deformation and deforms more or less uniformly as a coherent tectonic block (Bennett et al., 2012).   We take advantage of these characteristics of the pro-wedge to model the catchment scale uplift as uniform, with a single

point of base level fall defined by the point where the river effectively meets sea level at the foreland or the coastline. Our treatment of uniform uplift does not extend to the entire Apennine range; in fact, the orogen-strike parallel distribution of catchments (**Fig. 2**) allows our analysis to explore non-uniform uplift for the northern, central, and southern Apennine regions.

310   Rocks exposed in the pro-wedge range from massively-bedded Mesozoic carbonates that have a low erodibility to medium-bedded carbonates and siliciclastics or chaotic melange with modest erodibility, to thinly-bedded and semi-consolidated sandstone, siltstone, and mudstone with a high erodibility. Lesser amounts of Messinian evaporites, ophiolite, igneous rocks, and alluvium round out the rock types.

315   The northern Apennine pro-wedge is a stack of several tectono-stratigraphic units that have built ~30 km thick crust over an intact Adriatic slab (Di Stefano et al., 2009; **Fig. 3**). At the top of this stack lie rocks of moderate and variable erodibility of the Ligurian nappe (**Fig. 3, unit 6**). Ligurian rocks overlie harder siliciclastic turbidites of the Cervarola and Macigno formations (**Fig. 3, unit 4**), and are overlain by epiligurian sandstone, marl, and mudstone of similar or

320   greater erodibility (**Fig. 3, units 1, 3**). Ligurian rocks dominate in the western portion of the northern Apennines whereas turbidites of the Marnoso Arenacea (**Fig. 3, unit 3**) dominate in the east. Ligurian rocks are again present in the valley of the Marecchia (**Fig. 3**) where the northern Apennines transition to the central Apennines. Northern Apennine rivers flow northward from a drainage divide at an elevation of ~900 m to the Po Plain base level (**Fig. 2.**, swath N-N') in

325   narrow, nearly parallel catchments.

     The central Apennine pro-wedge, in contrast, is a stack of mostly Mesozoic-early Cenozoic carbonates and middle-late Cenozoic mixed carbonate-siliciclastic rocks ~30 km thick over an intact Adriatic slab (**Fig. 4**). This stack is floored by a low-angle detachment, the Alto-Tiburina fault (ATF; Barchi et al., 1998; Pialli et al., 1998) that controls the transition from shortening in

330   the pro-wedge to extension in the retro-wedge (**Fig. 4b**). As the crust is actively being thinned by the ATF some measure of dynamic support is envisioned to explain the topography of the central Apennines (Facenna et al., 2014). Low erodibility carbonates tend to underlie anticlinal ridges (**Fig. 4**, **units 5 and 12**) whereas the intervening synclines are floored by softer siciliclastics and marls (**Fig. 4**, **units 2 and 3**). From north to south in the central Apennines, distinct anticlinal

335   ridges coalesce into a large, massive carbonate platform that is cut by active normal faults (**Fig.**

11

4). Most of the rivers in the central Apennines flow in narrow parallel catchments with both strike parallel and transverse segments. The rivers draining the large carbonate platform in the southern part of the central Apennines have a rectilinear pattern probably structurally influenced by extensional basins.   Central Apennine rivers flow from the drainage divide at elevations of

340   ~800 – 1000 m, reaching base level at the Adriatic coastline (**Fig. 2.**, swath C-C').

The southern Apennines cover a wide region of mostly extended, and thinned crust detached from the Adriatic slab in comparison to the central and northern Apennines (**Figs. 2, 5**). Rocks of Ligurian affinity (**Fig. 5**, unit 6), with an epi-Ligurian cover (**Fig. 5**, units 2, 3) are detached from underlying imbricate carbonates (Mazzoli et al., 2008; 2014; **Fig. 5b**). Closer to the plate

345   boundary, Cenozoic marls and siliciclastic rocks have also been incorporated into the wedge; however, there is no evidence for continued subduction at the plate boundary in the Bradonic Trough. As a result, dynamic support above a detached Adria slab is generally viewed as necessary to support southern Apennine topography (**Fig. 2**, swaths Sn-Sn' and Ss-Ss'; Faccenna et al., 2014). Southern Apennine catchments have dendritic to rectilinear headwaters at

350   elevations of ~900 m that progressively narrow to parallel trunk valleys as the streams reach base level defined by the Adriatic coast or the foreland plain (**Fig. 2**, swaths Sn-Sn' and Ss-Ss').

METHODS: THE MODELING DATASET AND LINEAR INVERSION APPROACH

We select ten pro-wedge catchments spanning nearly the entire length of the Apennines

355   except for Calabria (**Fig. 2**) based on previous studies that have established the catchment-wide erosion rate, trunk channel incision rate, or both (**Table 1**). A 10-m DEM (TINITALY, Tarquini et al., 2007) is used to assemble the topographic data.   From north to south, these catchments are the Taro, Reno, Marecchia, Metaro, Esino, Chienti, Tronto, Pescara, Trigno, and Basento and they can be organized into northern (Taro, Reno, Marecchia; **Fig. 3**), central (Metaro, Esino,

360   Chiento, Tronto; **Fig. 4**), and southern (Pescara, Trigno, and Basento; **Fig. 5**) groups according to their geology and where they fall above proposed intact or detached slabs (Faccenna et al., 2014; **Fig. 2**). From a fixed topography reference frame, the mouths of these rivers are expected to lengthen whereas the headwaters are expected to contract due to the foreland translation of the drainage divide as rocks are advected westward through the wedge (Mayer et al., 2003; Buscher

365   et al, 2016). Evidence of drainage captures and reversal of Adriatic flank drainage westward to

the Tyrrhenian flank (and visa-versa) are evident in many all of the catchments and the growth of drainage area by basin spill-over and integration is present in others so the modeled uplift rates will presumably be influenced by these changes that will impact the slopes of χ-z plots (**Fig. 1**) if the integration is large and impulsive (c.f. Forte and Whipple, 2018).

370   Erosion and/or trunk channel incision rates and stream steepness are the two fundamental observables in the catchments (**Table 1**).   Erosion and incision rates are assembled from orogenic-scale mass balances (Bartolini et al., 1996), [10]Be terrestrial cosmogenic nuclide concentrations in alluvial sediment (Cyr and Granger, 2008; Ascione et al., 2012; Wittmann et al., 2016; Erlanger, 2019; this paper, **S1**), geomorphic terrane analysis (Tu, Ciccacci et al., 1986;

375   Guerra and Lazzari, 2020), modern sediment budgets (Faronni et at., 2001), and geomorphic markers (Picotti and Pazzaglia, 2008; Wegmann and Pazzaglia, 2009; Wilson et al., 2009; Coltorti et al., 1991; Gentile et al., 2017; Ascione et al., 2008; Amato et al., 2017; Nesci et al., 2012; Sembroni et al., 2020).

The mean reference channel concavity (θ_{ref}) for all ten catchments is calculated to be 0.47.

380   For a uniform catchment erosion rate, k_{sn} would be expected to scale linearly with rock erodibility (eq. 5) and a comparison to geology shows local variations at map contacts (Cyr et al., 2014; **Fig. 6**).   However, unsteady rock uplift (base level fall) at the river mouth will introduce transient waves of erosion in the form of knickpoints that migrate up-channel modifying stream steepness independent of rock type. The celerity of these erosional waves is controlled by both

385   the upstream drainage area and erodibility (eq. 6d).   So collectively, the catchment-wide distribution of k_{sn} reflects both the base level fall history, and changes in rock erodibility.

A goal in the channel inversion method is to account for the rock-erodibility component in k_{sn} (Gallen, 2018; Gailleton et al., submitted) so that remaining variations in stream steepness, discretized in χ (eq. 7), could be used to reconstruct the base level fall history from the transient

390   erosional waves. This goal is accomplished by using a geologic map shapefile to define domains of common rock erodibility where the mean value of k_{sn} could be calculated.   There is no predetermined assumption of relative rock erodibility, only that one rock type has a different erodibility than an adjacent type based on some textural, bedding, or compositional difference that are ultimately reflected in the lithostratigraphic units depicted on a geologic map. Using eq.

395   (5), the K value can be directly calculated for these domains and mapped onto the channels,

allowing for variable erodibility to be factored into the integration calculating response time (eq. 6d), steady-state channel elevation (eq. 8), or the discretization matrix for the linear inversion (eq. 9 below).

400   We use the 1:500,000 geologic map of Italy (http://sgi2.isprambiente.it/arcgis/services /servizi/cartageologica500k/MapServer/WmsServer) and group common geologic units into 10 rock erodibility categories (**Table 2, Figs. 3, 4, and 5; S2**). The relative erodibilities generally conform to assumptions of lithostratigraphic unit hardness, such as massive limestone being harder than bedded limestones, which are harder than turbiditic clastics, and poorly-consolidated clastics.

405   We begin the inversion process for all channels in a watershed using eq. (8) by discretizing z and χ values into spatial domains defined by rock-type (Gallen, 2018). Eq (8) is discretized into 'q' spatial domains by rock-type (q = number of domains). The elevation at any point along the river profile is the product of k_{sn} and change in χ at each stream node below. These data can be organized into matrix form

410

$$A * k_{sn} = z \qquad (9),$$

where $A*$ is an n by q matrix (number of stream nodes by number of domains) of the change in χ at each stream node. The k_{sn} and z matrices are n by 1 arrays of their respective parameters. The
415   matrix solution for k_{sn} is an over-determined inverse problem. To solve for k_{sn}, the method involves a non-negative least squares regression to determine the best-fit k_{sn} values that best reproduce the observed elevation in each rock-type domain.

    The rock erodibility values (K) are then calculated in each catchment domain using the best fit k_{sn}, basin averaged erosion rate, and their respective uncertainties in eq (5) using a monte carlo
420   routine with 1000 iterations (Gallen, 2018). However, in order to compare inverted uplift histories between multiple basins, a consistent set of erodibility values for each rock-type need to be averaged across all ten catchments. Uncertainties in k_{sn} and E are propagated to K using

$$\frac{\Delta K}{K} = \sqrt{\left(\frac{\Delta E}{E}\right)^2 + \left(\frac{\Delta k_{sn}}{k_{sn}}\right)^2} \qquad (10),$$

425

the weighted mean K value (K_{wtd}) follows from

$$K_{wtd} = \frac{\sum n_i K_i}{\sum n_i}$$

(11),

430

where n_i is the number of nodes for a particular rock domain, and the standard error on K_{wtd} is calculated using

$$SE(K_{wtd}) = \sqrt{\frac{\sum n_i^2 * var(K_i)}{(\sum n_i)^2}}$$

435

(12),

where $var(K_i)$ is equal to $K_{wtd}^{0.5}$. These rock-type specific K values result in a τ-z plot (**S3**) that has much less scatter than a typical χ–z plot because the former specifically accounts for the contribution of rock erodibility in the observed k_{sn}, whereas the latter tends to average across
440 these differences at the catchment scale. Lastly, these rock-type specific τ values are input into a slightly modified linear inversion scheme (Goren et al., 2014) where this K specific τ replaces a given number of time intervals to determine what z values correspond to a given time step. We output the τ-z plots use a uniform time step of 0.25 Myrs. The models are run in Matlab using Matlab scripts (**S4;** https://github.com/sfgallen/Block_Uplift_
445 Linear_Inversion_Models) that utilize Topotoolbox (Schwanghart and Scherler, 2014) and Topographic Analysis Kit (Forte and Whipple, 2019) Matlab tools.

RESULTS

    A general pattern of rock uplift is shown in the mean model k_{sn} (**Table 1**) and k_{sn} maps (**Figs.**
450 **3, 4, 5, 6**). The three northern catchments have k_{sn} values ~50-60 $m^{0.96}$. The central catchments show a distinct gradient in k_{sn} values from that doubles from ~50 to ~100 $m^{0.96}$ towards the south, and the increase in k_{sn} coincides with the proposed boundary with the detached slab (**Fig. 2,** between the Chienti and Tronto catchments). The three southern catchments show uniformly high k_{sn} values ~100 $m^{0.96}$.

455   Accounting for non-uniform erodibility impacts the recovered rate of base level fall history
(**Fig. 3c and d**). As a representative example, the uplift history for the Reno catchment varies in
both response time and uplift rate when modeled using a uniform rock erodibility corresponding
to the mean k_{sn} value (**Fig. 3d**) in comparison to the model that considers variable erodibility
(**Fig. 3c**). In general, accounting for a variable rock type tends to increase the variability in U
460   between model time steps, and also to reduce the deceleration of uplift rate towards the present.
This occurs because the low k_{sn} values near catchment mouths reflect the soft Plio-Pleistocene
rocks that commonly outcrop in that part of the catchment. The uniform erodibility model
expresses these low k_{sn} values, that are below the catchment mean, as slow uplift rates. Similarly,
variable U for long response times in the τ-U plots for the Reno and all catchments (**Fig. 3c**)
465   probably reflect large changes in first-order stream steepness as those channels approach the
catchment divide.

   The modeled rate of base level fall for a catchment (τ-U plots) are consistent with their
corresponding χ–z plots when τ is mapped into the χ–z plots using the relationship between
response time and elevation (**S3**). The τ-U plots are further consistent with the general trends in
470   stream steepness for the northern, central, and southern Apennine catchment groups. In this
analysis, we consider only that part of the rate of base level fall history where the variability
expressed in the monte carlo models is $\leq \pm 0.1$ mm/yr (**Fig. 3c, 4c, 5c**, red vertical line). As a
result, we display and compare only the last 3 Ma of base level fall, even though some basins
have maximum response times > 3 Ma. The three northern basins show a trend of base level fall
475   commencing earlier in the west (**Fig. 3c Taro in comparison to Fig. 3c Marecchia**) . The onset
of uplift rapidly rises to rates of ~0.5-0.6 mm/yr which is maintained in the Taro, but diminishes
in both the Reno and Marecchia. The χ-z plots for the Taro and Reno catchments are generally
linear, the trunk channel lines not withstanding, and consistent with an approximately steady rate
of base level fall since emergence of the northern Apennines. The gentle concavity in the Reno
480   χ-z plot after 1.5 Ma is reflected in the gently diminishing rate of base level fall from ~0.5 to 0.3
mm/yr (**Fig. 3c, Reno**). In contrast, the rate of base level fall and χ-z plot for the Marecchia
catchment (**Fig. 3c Marecchia**) are dominated by tributaries to the main channel that are gently
concave since 1.75 Ma when the catchment was impulsively uplifted.

The catchments in the central Apennines share common base level fall histories older than 1 Ma, and then diverse histories since 1 Ma (**Fig. 4c, d**). Specifically, the catchments indicate that they were uplifted at ~2.75 – 2.25 Ma, first in the north and more recently in the south. Once emergent, they experienced a relatively steady, or gently diminishing rate of base level fall until 1 Ma. At 1 Ma, the Metaro, Esino, and Chienti catchments experienced an impulsive increase in the rate of base level fall, that has since diminished towards the present (**Fig. 4c**). Although geologically similar, the base level fall history for the Tronto catchment since 1 Ma is different, showing an impulsive uplift to rates of 0.8 mm/yr, followed by deceleration to 0.3 mm/yr (**Fig. 4c**, Tronto). The change in rate of base level fall for all four catchments that occurs at 1 Ma is expressed in the kinked χ-z plots where the segment older than 1 Ma is nearly linear, whereas the segment younger than 1 Ma is steep, tapering off to a concave shape towards the present.

For the southern Apennines, emergence and stabilization of the catchments is older for the Pescara at ~3 Ma, and youngest for the most southern catchment, the Basento, at ~1.75 Ma (**Fig. 5c**). The record for the Trigno is a bit problematic because of the high variability in the monte carlo simulations older than 2 Ma, but it shares a common pattern with the Pescara and Basento expressed as an acceleration in the rate of base level fall beginning at ~2 Ma at rates of ~0.2 – 0.3 mm/yr to rates of ~0.6-0.8 mm/yr which is 2x greater than the rates expressed in the τ-U plots for the northern and central Apennines. Decreases in the rate of base level fall is nearly symmetrical for the Pescara catchment, but asymmetric for both the Trigno and Basento catchments (**Fig. 5c**). The trunk channels are segmented in the χ-z plots and indicate complicated integration of the catchment and all of its tributaries (**Fig. 5d**). Of note, the S-shaped χ-z plots for the Pescara and Basento catchments contrast with the mostly linear χ-z plot of the Trigno catchment (**Fig. 5d**).

DISCUSSION

The reconstructed base level fall histories of the ten catchments analyzed in this study indicate non-uniform and unsteady uplift of the Apennines at the scale of the entire orogen, not consistent with a single synchronous tectonic or dynamic uplift process (**Fig. 7**). Furthermore, the segmented and complex relationships between the trunk channels and tributaries expressed in many of the χ-z plots (**Figs. 3d, 4d, 5d**) suggest that the uplift may also not be uniform at the

17

catchment scale, and/or area-growing drainage integration or area-diminishing drainage captures

515 have occurred in the past 3 Ma. We discuss these findings, all of which are consistent with what is already known about the geologic and geomorphologic development of the Apennines, in the context of the three models for transverse drainage development.

We interpret these results first in terms of catchment-scale changes in tectonic or dynamic processes that drive base level fall at the mouth of the catchment, but are allowed to vary along

520 strike parallel to the orogen. Secondly, we modify those base level fall interpretation in terms of the possible complicating factors introduced by local fault-controlled base level fall within the catchment as well as gains or losses of drainage area. The process driving base level change can be inferred by comparisons of the τ-U plots to regional topographic (Coltorti and Pieruccini, 2000; D'Agostino et al., 2001; Bartolini et al., 2003; Ascione et al., 2008), geomorphic marker

525 (Coltorti et al., 1991; Picotti and Pazzaglia, 2008; Wegmann and Pazzaglia, 2009; Wilson, 2009; Nesci et al., 2012), geologic (Pizzi, 2003; Gunderson et al., 2018), sedimentologic (Bartolini et al., 1996; Cosentino et al., 2017), thermochronologic (Thomson et al., 2010; Mazzoli et al., 2008), and isotopic (San Jose et al., 2020) evidence. A general conclusion of this comparison is that the rock and surface uplift of the Apennines is a recent development in the otherwise long

530 history of tectonic assembly of the orogen. Most of the Apennines emerged in the Pliocene and rapidly grew to a rugged mountain range in the Pleistocene (**Fig. 7**); however, the processes fueling that emergence and growth vary along the length of the orogen.

In the northern Apennines, the Taro, Reno, and Marecchia catchments have a base level fall history most consistent with growth and isostatic emergence of the orogenic wedge atop an intact

535 Adriatic slab (DiStefano et al., 2009; Benoit et al., 2011; Faccenna et al., 2014; **Figs. 3, 7a**). Several studies (Basili and Barba, 2007; Picotti and Pazzaglia, 2008; Bennett et al., 2012; Gunderson et al., 2018) and recent seismicity (Lavecchia et al., 2012) point to ongoing, but decelerating convergence for this part of the range. The abrupt base level fall modeled for these catchments at ∼ 2 – 1.5 Ma is temporally coincident with the slowing of shortening at the toe of

540 the Apennine wedge beneath the Po foreland, and the initiation of a crustal-scale, thick-skinned pedi-Apenninic fault (Boccaletti et al., 1985) at the location of the current mountain front. Slip on that fault appears to dominate uplift and fluvial incision at the mountain front by ~1 Ma (Picotti and Pazzaglia, 2008; Wegmann and Pazzaglia, 2009; Wilson, et al., 2009; Gunderson et

18

al., 2018) which we interpret to be recorded in the long profiles by approximately steady rates of
uplift at ~0.4 mm/yr. These modeled rates of base level fall are similar to those constructed from
thermochronology (Thomson et al., 2010), incision rates derived from terraces (Picotti and
Pazzaglia, 2008; Wegmann and Pazzaglia, 2009; Wilson, et al., 2009; Ponza et al., 2010), and the
basin wide erosion rates (Table 1). Collectively, these data indicate that tectonic processes are
balanced by surface processes in the northern Apennines.

The combination of loss of drainage area in the headwaters and local fault offset in the
northern Apennine catchments modify, but do not obscure the base level fall introduced at the
catchment mouth by the pedi-Apenninic fault. For example, the impulsive base level fall for the
Marecchia catchment at 1.75 Ma, followed by progressive decay in the rate of uplift is consistent
with a major drainage capture event for that catchment (**Figs. 1c, 3, and C in Fig. 7a**).
Nevertheless, the rates of overall base level change for the Marrecchia is similar to the Taro and
Reno. Similarly, the Taro and Reno τ-U plots show a gentle increase in base level fall at 1 Ma
that could be the result of expected headwater drainage loss (**Figs. 1a, 3, and P in Fig. 7a**), but
the change in rate is small and does little to change the overall trend. Evidently, shortening,
faults, and fold growth accompanied rock uplift in the northern Apennines over the past 2 Ma
and the rivers have been able to maintain parallel courses to the Po foreland, carving valleys
transverse to structure (**Figs. 3, and 6**), even though this part of the range lacks the narrow
gorges carved through hard limestone ridges like those present further south in the central and
southern Apennines. Considering the mean τ-U, χ-z, and cumulative base level fall plots (**Fig. 7a**) uplift in the northern Apennine catchments are best explained by the isostatic response to
crustal thickening, where transverse rivers are formed following the the Mazzanti and Trevisan
(1978) and Alvarez (1999) models (**Fig. 1a**).

Further south, the Metaro, Esino, Chienti, and Tronto catchments in the central Apennines
show a progressive transition from uplift dominated by shortening, wedge growth, and isostasy
in the north where the slab is intact (**Fig. 2**), to dynamic support and regional uplift where the
Adriatic slab is envisioned to have torn or delaminated, forming a slab window further south
(Piromallo and Morelli, 2003; DiStefano et al., 2009; Faccenna et al., 2014). Modeled base level
fall rates for the Metaro, Esino, and Chienti catchments are approximately steady after these
catchments emerged impulsively at ~3 Ma (**Fig. 7b**). The base level fall history for the Tronto is

markedly different in magnitude, timing, and shape. Notably, the Tronto is located south of the

575   proposed location of the slab window (Faccenna et al., 2014; **Fig. 2**).

The evidence for active shortening in the wedge and the confines of a catchment is less clear for the central Apennines (Hreinsdottir and Bennett, 2009; Bennett et al., 2012) in comparison to the northern Apennines, and the geologic evidence would suggest that most active folding ceased in the late Pliocene (Pizzi, 2003). However, continued local fold growth is evident in the

580   mapped relationships of Plio-Pleistocene strata (ie. Turco et al., 2009) and in middle-late Pleistocene uplifted and warped terraces (Wegmann and Pazzaglia, 2009). As with the northern Apennines catchments, the Mazzanti and Trevisan (1978) and Alvarez (1999) models for transverse drainages mostly applies in the central Apennines for the Metaro, Esino, and Chienti catchments primarily in the way that it predicts the location of the modern channels as being

585   inherited from ancestral sediment routing pathways (Scarselli et al., 2006) and in the steadiness of the uplift rate. We interpret a two-stage history for the central Apennines as reflected in the τ-U plots, segmented χ-z plots (**Figs. 4, 7b**), and dissected upland, low-relief paleovalleys (**Fig. 2**, cross-sections X-X', Y-Y'; Alvarez, 1999).   The first stage is dominated by crustal-thickening driven isostatic uplift in the late Pliocene and early-Pleistocene during shortening and wedge

590   growth. It is during this phase that the Mazzanti and Trevisan (1978) and Alvarez (1999) transverse drainage mechanism dominates (**Fig. 1a**). Subsequent to that and increasing in magnitude to the south, a second phase of uplift has been driven by dynamic processes and regional surface uplift in the middle Pleistocene at ~0.75 – 1 Ma. During this second phase a catchment-wide superposition mechanism dominates transverse drainage development to deepen

595   gorges already fixed during the first phase (**Fig. 1b**). This two-phased approach to the formation of transverse drainages in the central Apennines aligns with the findings of other river channel studies that appeal to two or more geologic and tectonic processes conspiring for the rivers to maintain their courses across the geologic structures (Mayer et al., 2003). Similar to the northern Apennines, modeled base level fall in the catchments of the central Apennines are similar in

600   magnitude to erosion and incision rates (**Table 1**).

Alternatively, the second phase of uplift ~0.75 – 1 Ma is not a dynamic contribution to base level fall, but rather indicates drainage capture or piracy in the headwaters of these central Apennine catchments (**C and P respectively in Fig. 7b**). The geomorphic evidence for piracy

and loss of drainage in the Metaro, Esino, and Chienti catchments is particularly strong as active normal faults bounding late and middle Pleistocene basins are present in the headwaters of these catchments (**Fig. 4**) and the entire region sits atop the ATF decollment. Furthermore, the eastward march of the extensional deformation front for this part of the range is well-described by the age of the extensional basins (Cavinato and DeCelles, 1990) and the similarity in the τ-U plots for the Metaro, Esino, and Chienti may be related to a major middle Pleistocene eastward-shift in the drainage divide and loss of headwater drainage. As with the northern Apennine catchments, these potential geomorphically-driven modifications of the overall τ-U, χ-z, and cumulative uplift plots are small compared to the overall trend of base level fall which has been relatively steady over the past 3 Ma, not considering the Tronto catchment (**Fig. 7b**).

Lastly, the Pescara, Trigno, and Basento catchments in the southern Apennines are located mostly in a zone of crustal extension and accordingly, show τ-U and χ-z plots consistent with the idea that this region has been experiencing syn-uplift extension in the past ~2 Ma, with an increase of that uplift in the past 1 Ma particularly evident in the Pescara and Basento catchments (**Fig. 7c**). Although part of the central Apennine catchments in this stu(Right)dy, the Tronto catchment has τ-U and χ-z plots more consistent with the three southern catchments (**Figs. 5, 7c**). In particular, the long-period, asymmetric growth in uplift rate to a peak ~ 0.5 Ma, and subsequent gentle decline is consistent with superposition of a pre-existing drainage transverse to underlying, formerly buried structures (**Fig. 1b**), driven by a dynamic process. The region of dynamically-driven regional uplift is located above the foundered Adriatic slab (Faccenna et al., 2014), the northern edge of which we would place between the Tronto and Chienti catchments (**Fig. 2**). The largest modeled rates of base level fall are derived from the southern Apennine catchments and at ~0.7-0.8 mm/yr for the past ~1 Ma are similar, if not somewhat less than what has been has been reported from other geologic, geomorphic, and thermochronologic studies that have argued for rates ~1-1.5 mm/yr (Pizzi, 2003, Amato et al., 2003; Mazzoli et al., 2008; 2014). The basin wide erosion rates for the southern basins (**Table 1**; Ascione et al., 2012) are lower than the river incision or uplift rates, indicating a more transient nature of the southern Apennine landscape in comparison to the central and northern parts of the range.

The problem of drainage area changes in the southern catchments inclusive of the Tronto may have a more significant impact on how to interpret the τ-U plots, with respect to the

21

northern and central catchments. For example, catchment growth by headward capture or overflow is known to be a dominant process for the Pescara (Geurts et al., 2018, 2020) and catchments adjacent to the Basento (Buscher et al., 2017). Impulse growth in drainage area due to a capture event is consistent with the spikes in uplift rate observed for the Basento and Pescara basins in the past 0.75 Ma (**Figs. 1c, 5, and C in Fig. 7c**). However, in summary, the overall *τ-U, χ-z,* and cumulative uplift plots for the catchments that are situated above the slab window have trends consistent with growing rates of uplift through the middle-late Pleistocene most consistent with transient, dynamic processes (**Fig. 7c**).

The modeled history of base level fall presented here represents one of the few ways in which surface uplift of a catchment can be independently determined from a geomorphic data set. Where datable geomorphic or stratigraphic markers such as river or marine terraces are lacking, surface uplift rates in the Apennines have been estimated from the remnants of low-relief erosional surfaces preserved primarily on hard, carbonate ridges (Coltorti and Pieruccini, 2000; Amato et al., 2003; Ascione et al., 2008) where the erosion rates are assumed to be very low. As a test to that assumption, San Jose et al (2020) measured and assembled paleo-elevation oxygen isotopic data from pedogenic carbonates preserved in extensional basins throughout the range. Their data show a -5 per mil isotopic shift caused by high elevation rainfall starting in the late Pliocene ~3 Ma for extensional basins at or east of the drainage divide, including those that are in the headwaters of several of the central and southern Apennine catchments modeled in this study. A similar isotopic shift is not observed for extensional basins in central Italy, well west of the drainage divide. The magnitude of the rainfall isotopic shift is consistent with 1–2 km of surface uplift of those basins, consistent with our modeled data (**Fig. 7**, cumulative uplift plots) and the assumption that Apennine upland surfaces are eroding slowly.

CONCLUSIONS

Linear inversion of longitudinal profile data provides an independent means to reconstruct the base level fall history of a catchment and test models for the development of rivers that flow transverse to structure. Under reasonable assumptions for catchment-wide uniform uplift, but non-uniform rock erodibility linked to major, mapped lithostratigraphic units, the observables of stream steepness (k_{sn}) and catchment erosion rate (E) can be used in a detachment-limited stream

power channel erosion rule framework where the power dependency on slope is 1 (n=1) to model the channel response time and its steady state elevation. Considering results when model simulation variability ≤ 0.1 mm/yr suggests that uplift and the carving of a transverse drainages commenced between 2 - 3 Ma for the entire orogen, but the main tectonic processes driving the uplift and geomorphic processes guiding the transverse channel incision vary along the length of the range. Isostatically-driven uplift in response to wedge shortening and thickening dominate the uplift processes for the northern Apennine catchments. Here, the transverse drainage model of Mazzanti and Trevisan (1978) generally applies. In the central Apennines where the Mazzanti and Trevisan (1978) model was first developed and later tested (Alvarez, 1999; Mayer et al., 2003) the uplift process transitions from wedge shortening in the north to dynamic mantle in the south with nearly a doubling of the uplift rate at the proposed location of a tear or slab window in the Adriatic slab (Faccenna et al., 2014). The base level fall histories for central Apennine streams, combined with the regional geomorphology of low-relief upland surfaces collectively argue for a two-phase tectonic process of transverse drainage development where the Mazzanti and Trevisan (1978) and Scarselli et al (2006) mechanisms locks the main valleys in place, followed by dynamic uplift that superimposes the channels across hard, previously buried anticlinal ridges (Alvarez, 1999). Rapid, dynamic uplift of the southern Apennines in the past ~ 1 Ma, coupled with drainage integration of rivers through a broad zone of crustal extension (Geurts et al., 2018; 2020; Buscher et al., 2017) conspire to generate the transverse drainages in this region. In summary, the rates of rock uplift modeled in this study, when integrated for surfaces or stratigraphic deposits that have not experienced any post-depositional erosion results in cumulative uplift ranging from ~900 m for the central Apennines to ~1800 m for the southern Apennines (**Fig. 7**), both consistent with recent, independent estimates of surface uplift from oxygen isotopic paleo-elevation studies (San Jose et al., 2020).

23

700

REFERENCES

Alvarez, W., 1999, Drainage on evolving fold-thrust belts: a study of transverse canyons in the
    Apennines: Basin Research, 11, 267-284.

705 Amato, A., Aucelli, P. P. C., and Cinque, A., 2003, The long-term denudation rate in the Southern
    Apennines chain (Italy): a GIS-aided estimation of the rock volumes eroded since middle
    Pleistocene times: Quateranry International, 101-102, 3-11.

Artoni, A., 2013, The Pliocene-Pleistocene stratigraphic and tectonic evolution of the central
    sector of the western Periadriatic basin of Italy: Marine and Petroleum Geology, 42, 82-
710   106.

Ascione, A., Cinque, A., Miccadei, E., Villani, F., and Berti, C., 2008, The Plio-Quaternary upift
    of the Apennine chain: new data from the analysis of topography and river valleys in
    central Italy: Geomorphology, 102, 105-118.

Ascione, A., Capalbo, A., Capolongo, D., Mazzoli, S., Pazzaglia, F. J., Valente, E., and Zattin,
715   M., 2012, Uplift vs. denudation in the southern Apennines: geomorphologic evidence and
    constraints from terrestrial cosmogenic nuclides and apatite (U-Th)/H data: Rend. Online
    Soc. Geol. It., Vol. 21 (2012), pp. 1102-1104.

Balley, A. W., Burbi, L., Cooper, C., and Ghelardoni, R., 1986, Balanced sections and seismic
    reflection profiles across the central Apennines: Memobrie della Societa Geologica
720   Italiana, 35, 257-310.

Barchi, M., De Feyter, A., Magnani, M., Minelli, G., Pialli, G., and Sotera, B., 1998, Extensional
    tectonics in the Northern Apennines (Italy): evidence from the CROP03 deep seismic
    reflection line, Mem. Soc. Geol. Ital., 52, 528–538, 1998.

Bartolini, C., 2003, When did the Northern Apennine become a mountain chain?: Quaternary International, v. 101-102, pp. 75-80.

Bartolini, C., Caputo, R. and Pieri, M., 1996, Pliocene–Quaternary sedimentation in the Northern Apennine Foredeep and related denudation: Geological Magazine, v. 133, pp. 255-273.

Bartolini, C., D'Agostino, N. A., and Dramis, F., 2003, Topography, exhumation, and drainage network evolution of the Apennines: Episodes, DOI: 10.18814/epiiugs/2003/v26i3/010.

Basili, R. and Barba, S., 2007, Migration and shortening rates in the northern Apennines, Italy: implications for seismic hazard: Terra Nova, 19, 462-468.

Bennett, R. A., Serpelloni, E., Hreinsdottir, S., Brandon, M. T., Buble, G., Basic, T., Casale, G., Cavaliere, A., Anzidei, M., Marjonovic, M., Minelli, G., Molli, G., & Montanari, A., 2012, Syn-convergent extension observed using the RETREAT GPS network, northern Apennines, Italy: Journal of Geophysical Research, 117, B04408, doi:10.1029/2011JB008744.. H., Torpeu, M., Liszewski, K., Levin, V., and Park, J., 2011, P and S wave upper mantle seismic velocity structure beneath the northern Apennines: New evidence for the end of subduction: Geochem. Geophys. Geosys., 12, Q06004, doi:10.1029/2010GC003428.

Benoit, M. H., M. Torpey, K. Liszewski, V. Levin and J. Park, 2011, P and S wave upper mantle seismic velocity structure beneath the northern Apennines: New evidence for the end of subduction: Geochemistry, Geophysics, Geosystems, 12, Q06004, doi:10.1029/2010GC003428, 2011.

Boccaletti, M., Corti, G., Martelli, L., 2011, Recent and active tectonics of the external zone of the Northern Apennines (Italy): International Journal of Earth Science, (Geologische Rundschau), 100, 1331-1348, DOI: 10.1007/s00531-010-0545-y.

Boccaletti, M., M. Coli, C. Eva, G. Ferrari, G. Giglia, A. Lazzarotto, A. Merlanti, F. Nicolich, R. Papani, and G. Postpischl, 1985, Considerations on the seismotectonics of the Northern Apennines: Tectonophysics, 117, 7 – 38.

Brocard, G., Willenbring, J., Suski, B., Audra, P., Authemayou, C., Cosenza-Muralles, B., Moran-Ical, S., Demory, F., Rochette, P., Vennemann, T., Holliger, K., and Teyssier, C., 2012, Rat and processes of river network rearrangement during incipient faulting: The case of the Cahabon River, Guatemala: American Journal of Science, 312, 449-507.

Buscher, J. T., Ascione, A., and Valente, E., 2016, Decoding the role of tectonics, incision and
755   lithology on drainage divide migration in the Mt. Alpi region, southern Apennines, Italy:
           Geomorphology, 276, 37-50, doi:10.1016/j.geomorph.2016.10.003.

Caporali, A., Barba, S., Carafa, M.M.C., Devoti, R., Pietrantonio, G., Riguzzi, F. 2011. Static
           stress drop as determined from geodetic strain rates and statistical seismicity: Journal of
           Geophysical Research, 116, B02410. doi:10.1029/2010JB007671.

760 Carminati, E., and Doglioni, C., 2012, Alps vs. Apennines: The paradigm of a tectonically
           asymmetric Earth: Earth Sci Rev, 112, 67-96.

Cavinato, G. P. and DeCelles, P., 1999, Extensional basins in the tectonically bimodal central
           Apennines fold-thrust belt, Italy. Response to corner flow above a subducting slab in
           retrograde motion: Geology, 27, 955–958.

765 Chiaraluce, L. Barchi, M. R., Carannante, S., Collettini, C., Mirabella, F., Pauselli, C., Valoroso,
           L., 2017,   The role of rheology, crustal structures and lithology in the seismicity
           distribution of the northern Apennines: Tectonophysics, 694, 2810-291.

Ciccacci, S., Fredi, P., Palmieri, E.L., and Pugliese, F., 1986, Indirect evaluation of erosion entity
           in drainage basins through geomorphic, climatic and hydrological parameters: Int.
770   Geomorphol., 2, 33–48.

Coltorti, M. and Pieruccini, P., 2000, A lat lower Pliocene planation surface across the Italian
           Peninsula: a key tool in neotectonic studies: Journal of Geodynamics, 29, 323-328.

Coltorti, M., Consoli, M., Dramis, F., Gentili, B., amd Pambianchi, G., 1991, Evoluzione
           geomorfologica delle piane alluvionali delle Marche centro-meridionali: Geogr. Fis.
775   Dinam. Quat., 14, 87-100.

Cosentino, D., Asti, R., Nocentini, M., Gliozzi, E., Kotsakis, T., Mattei, M., Esu, D., Spadi, M.,
           Tallini, M., Cifelli, F., Pennacchioni, M., Cavuoto, G., Di Fiore, V., 2017, New insights
           into the onset and evolution of the central Apennine extensional intermontane basins
           based on the tectonically active L'Aquila Basin (central Italy): Geol. Soc. Am. Bull., 129,
780   1314–1336. https://doi .org /10 .1130 /B31679 .1.

Cyr, A., Granger, D. E., Olivetti, V., and Molin, P., 2014, Distinguishing between tectonic and
           lithologic controls on bedrock channel longitudinal profiles using cosmogenic [10]Be
           erosion rates and channel steepness index: Geomorphology, 209, 27-38.

Cyr, A.J., Granger, D.E., 2008, Dynamic equilibrium among erosion, river incision, and coastal
uplift in the northern and central Apennines, Italy: Geology, 36, 103–106.

Cyr, A.J., Granger, D.E., Olivetti, V., Molin, P., 2010, Quantifying rock uplift rates using channel
steepness and cosmogenic nuclide-determined erosion rates: examples from northern and
southern Italy: Lithosphere 2, 188-198.

D'Agostino, N., Jackson, J. A., Dramis, F., Funiciello, R., 2001, Interactions between mantle
upwelling, drainage evolution and active normal faulting: an example from the
central Apennines (Italy): Geophysical Journal International, 147, 475-497.

Davis, W.M., 1889, Rivers and valleys of Pennsylvania: National Geographic, v. 1, p. 183–253.

Devoti, R., Riguzzi, F., Cuffaro, M., & Doglioni, C., 2008, New GPS constraints on the
kinematics of the Apennines subduction: Earth and Planetary Science Letters, 273, 163–
174.

Di Stefano, R., Kissling, E., Chiarabba, C., Amato, A., and Giardini, D., 2009, Shallow
subduction beneath Italy: Three-dimensional images of the Adriatic-European-Tyrrhenian
lithosphere system based on high-quality P wave arrival times: Journal of Geophysical
Research, 114, B05305, doi:10.1029/2008JB005641.

Doglioni, C., Harabaglia, P., Merlini, S., Mongelli, F., Peccerillo, A.T., Piromallo, C., 1999,
Orogens and slabs vs. their direction of subduction: Earth Science Reviews, 45, 167–208.

Douglass, J., Meek, N., Dorn, R., and Schmeeckle, M. W., 2009, A criteria-based methodology
for determining the mechanisms of transverse drainage development, with application to
the southwestern United States: Geological Society of America Bulletin, 121, 586-598.

Elter, P., Giglia, G., Tongiorgi, M. and Trevisan, L.,1975, Tensional and compressional areas in
the recent (Tortonian to present) evolution of the Northern Apennines. Boll: Geofis.
Teorica Applicata, 17, 3–18.

Erlanger, E., 2019, Erosion and weathering of the northern Apennines with implications for the
tectonics and kinematics of the orogen: ETH Zurich, Doctoral Dissertation, 201 p.

Faccenna, C., Becker, T. W., Miller, M. S., Serpelloni, E., Willett, S. D., 2014, Isostasy, dynamic
topography, and the elevation of the Apenninees of Italy: Earth and Planetary Science
Letters, 407, 163-174.

Farroni, A., Magaldi, D., and Tallini, M., 2002, Total sediment transport by rivers of Abruzzi (Central Italy): prediction with the RAIZAL model: Bull. Eng. Geol. Env, 61, 121-127.

815   Forte, A. M. and Whipple, K. X., 2018, Criteria and tools for determining drainage divide stability: Earth and Planetary Science Letters, 493, 102 - 117, doi:10.1016/j.epsl.2018.04.026.

Forte, A. M. and Whipple, K. X., 2019, Short commnication: The Topographic Analysis Kit (TAK) for Topotoolbox: Earth Surface Dynamics, 7, 87-95.

820   Gallen, S. F., 2018, Lithologic controls on landscape dynamics and aquatic species evolution in post-orogenic mountains: Earth and Planetary Science Letters, 493, 150-160.

Gentile, B., Pambianchi, G., Aringoli, D., Materazzi, M., and Giacopetti, M., 2017, Pliocene-Pleistocene geomorphological evolution of the Adriatic side of central Italy: Geologica Carpathica, 68, 1, 6-18.

825   Geurts, A. H., Whittaker, A. C., Gawthorpe, R. L., and Cowie, P. A., 2020, Transient landscape and stratigraphic responses to drainage integration in the actively extending central Apennines: Geomorphology, 353, https://doi.org/10.1016/j.geomorph.2019.107013.

Geurts, A.H., Cowie, P.A., Duclaux, G., Gawthorpe, R.L., Huismans, R.S., Pedersen, V.K.,Wedmore, L.N.J., 2018, Drainage integration and sediment dispersal in active
830   continental rifts: a numerical modelling study of the central Italian Apennines: Basin Res. 30 (5), 965–989.

Ghisetti, F., Vezzani, L., 2002, Normal faulting, transcrustal permeability and seismogenesis in the Apennines (Italy): Tectonophysics, 348, 155–168.

Gilbert, G. K., 1877, Report on the geology of the Henry Mountains [Utah], Washington, DC:
835   Publication of the Powell Survey, US Government Printing Office, 160 p.

Glotzbach, C., 2015, Deriving rock uplift histories from data-driven inversion of river profiles: Geology, 43, 467-470, doi:10.1130/G36702.1.

Goren, L., Fox, M., Willett, S.D., 2014, Tectonics from fluvial topography using formal linear inversion: theory and applications to the Inyo Mountains, California: J. Geophys. Res.,
840   Earth Surf., 119, 1651–1681, https://doi .org /10 .1002 /2014JF003079.

Guerra, V. and Lazzari, M., 2020, Geomorphic approaches to estimate short-term erosion rates: An example from Valmarecchia River system (Northern Apennines, Italy): Water, 12, 2535, doi: 10.3390/w12092535.

Gunderson, K. L., Anastasio, D, J., Pazzaglia, F. J., and Kodama, K. P., 2018, Intrinsically variable blind thrust faulting: Tectonics, 37, https://doi.org/10.1029/2017TC004917.

Hack, J. T. 1957. Studies of longitudinal stream profiles in Virginia and Maryland. U.S. Geological Survey Professional Paper. 294-B:45-97.

Hill, K., Hayward, A. 1988, Structural constraints on the Tertiary plate tectonic evolution of Italy: Marine and Petroleum Geology, 5, 2 – 16.

Howard, A. D., 1994, A detachment-limited model of drainage basin evolution: Water Resources Research, 30, 2261–2285.

Hreinsdottir, S. and Bennett, R. A., 2009, Active aseismic creep on the Alto Tiberina low-angle normal fault, Italy: Geology, 37, 683-686.

Johnson, D., 1931, Stream Sculpture on the Atlantic Slope: Columbia University Press, doi:https://doi.org/10.7312/john92980.

Kirby, E. and Whipple, K. X., 2012, Expression of active tectonics in erosional landscapes: Journal of Structural Geology, 44, 54–75.

Lague, D. 2013, The stream power river incision model: evidence, theory and beyond: Earth Surface Processes and Landforms, doi:10.1002/esp.3462.

Lavé, J., Avouac, J. P., 2001, Fluvial incision and tectonic uplift across the Himalayas of central Nepal, Journal of Geophysical Research 106, 26,561-26,591.

Lavecchia, G., Brozzetti, F., Barchi, M., Menichetti, M. & Keller, J.V., 1994, Seismotectonic zoning in east-central Italy deduced from an analysis of the Neogene to present deformations and related stress fields: Geological Society of America Bulletin, 106, 1107–1120.

Lavecchia, G., de Nardis, R., Cirillo, D., Brozzetti, F., and Boncio, P., 2012, The May-June 2012 Ferrara Arc earthquakes (northern Italy): Structural control of the spatial evolution of the seismic sequence and of the surface patter of coseismic fractures: Annals of Geophysics, 55: doi:10.4401/ag-6173.

870   Le Pichon, X., G. Pautot, J. M. Auzende, Olivet, J. L. 1971. La Mediterranee occidentale depuis l'oligocene; scheme d'evolution: The western Mediterranean since the Oligocene; evolutionary scheme, Earth and Planetary Science Letters, 13, 145 – 152.

Mayer, L., Menichetti, M., Nesci, O., and Savelii, D., 2003, Morphotectonic approach to the drainage analysis in the north Marche region, central Italy: Quaternary International, 101-
875   102, 157-167.

Mazzanti, R. and Trevisan, L., 1978, Evoluzione della rete idrografica nell'Appennino centro-settentrionale: Geograf. Fisica e Dinamica Quaternaria, 1, 55–62.

Mazzoli, S., D'Errico, M., Aldega, L., Corrado, S., Invernizzi, C., Shiner, P., and Zattin, M., 2008, Tectonic burial and "young" (<10 Ma) exhumation in the southern Apennines fold-
880   and-thrust belt (Italy): Geology, 36, 243-246.

Mazzoli, S., Ascione, A., Buscher, J. T., Pignalosa, A., Valente, E., and Zattin, M., 2014, Low-angle normal faulting and focused exhumation associated with late Pliocene change in tectonic style in the southern Apennines (Italy): Tectonics, 33, 1802–1818, doi:10.1002/2014TC003608.

885   Meek, N., 1989, Geomorphic and hydrologic implications of the rapid incision of Afton Canyon, Mojave Desert, California: Geology, v. 17, p. 7–10, doi: 10.1130/0091-7613(1989)017<0007:GAHIOT>2.3.CO;2.

Meek, N., and Douglass, J.C., 2001, Lake-overfl ow: An alternative hypothesis to explain Grand Canyon incision and development of the Colorado River, *in* Young, R.A., and Spamer,
890   E.E., eds., Colorado River origin and evolution: Grand Canyon, Grand Canyon Association, p. 199–204.

Meyerhoff, H. A. and Olmstead E. W., 1936, The origins of Appalachian drainage: Am. Jour. Sci., v. 232, p. 21-42.

Mudd, S. M., Clubb, F. J., Gailleton, B., and Hurst, M. D., 2018, How concave are river
895   channels?: Earth Surface Dynamics, 6, 505-523.

Nesci, O., Savelli, S., and Troiani, F., 2012, Types and development of stream terraces in the Marche Apennines (central Italy): a review and remarks on recent appraisals: Geomorphologie: relief, processs, environnement, 2, 215-238.

Oberlander, T., 1965, The Zagros stream: A new interpretation of transverse drainage in an orogenic zone: Syracuse, University of Syracuse, 168 p.

Perron, J. T. and Royden, L. 2013, An integral approach to bedrock river profile analysis: Earth Surface Processes and Landforms, 38, 570–576.

Piana Agostinetti, N., Steckler, M.S., Lucente, F.P., 2009, Imaging the subducted slab under the Calabrian Arc, Italy, from receiver function analysis: Lithosphere 1,131–138. http://dx.doi.org/10.1130/L49.1.

Picotti, V., and Pazzaglia, F. J., 2008, A new active tectonic model for the construction of the Northern Apennines mountain front near Bologna (Italy): J Geophys Res, 113, B08412, doi: 10.1029/2007JB005307.

Piromallo, C., Morelli, A., 2003, P-wave tomography of the mantle under the Alpine–Mediterranean area. J. Geophys. Res. 108 (B2), 2065.

Pialli, G., Barchi, M., and Minelli, G., 1998, Results of the CROP 03 deep seismic reflection profile: Mem. Soc. Geol. Ital., 52, 647 p.

Pizzi, A., 2003, Plio-Quaternary uplift rates in the outer zone of the central Apennines fold-and-thrust belt, Italy: Quaternary International, 101-102, 229-237.

Playfair, J., 1802, Illustrations of the Huttonian theory of the Earth: London, Cadell and Davis and Edinburgh, Creech; reprinted 1964: New York, Dover Publications, 528 p.

Pondrelli, S., Salimbeni, S., Ekstrom, G., Morelli, A., Gasperini, P. Vannucci, G., 2006, The Italian CMT dataset from 1977 to the present: Physics of the Earth and Planetary Interiors, 159, 286–303, doi:10.1016/j.pepi.2006.07.008.

Ponza, A., Pazzaglia, F. J., and Picotti, V., 2010, Thrust-fold activity at the mountain front of the northern Apennines (Italy) from quantitative landscape analysis: Geomorphology, 123, 211-231.

Prince, P. S., Spotila, J. A., and Henika, W. S., 2010, New physical evidence of the role of stream capture in active retreat of the Blue Ridge escarpment, southern Appalachians: Geomorphology, 123, 305-319.

Pritchard, D., Roberts, G. G., White, N. J., Richardson, C. N., 2009, Uplift histories from river profiles: Geophys. Res. Letters, 36, https://doi .org /10 .1029 /2009GL040928.

Royden, L., 1993, Evolution of retreating subduction boundaries formed during continental collision: Tectonics, 12, 629-638.

930 San Jose, M., Caves Rugenstein, J. K., Cosentino, D., Faccenna, C., Fellin, M. G., Ghinassi, M., and Martini, I., 2020, Stable isotope evidence for rapid uplift of the central Apennines since the late Pliocene: Earth and Planetary Science Letters, 544, https://doi.org/10.1016/j.epsl.2020.116376.

Scarselli, S., Simpson, G. D. H., Allen, P. A., Minelli, G., and Gaudenzi, L., 2007, Association
935 between Messinian drainage network formation and major tectonic activity in the Marche Apennines (Italy): Terra Nova, 19, 74-81.

Schwanghart, W., Scherler, D., 2014, Short communication: TopoToolbox 2 – MATLAB-based software for topographic analysis and modeling in Earth surface sciences: Earth Surf. Dyn.2, 1–7. https://doi .org /10 .5194 /esurf -2 -1 -2014.

940 Seeber, L., Gornitz, V., 1983, River profiles along the Himalayan Arc as indicators of active tectonics: Tectonophysics, 92, 335-367.

Sembroni, A., Molin, P., Soligo, M., Tuccimei, P., Anzalone, E., Billi, A., Franchini, S., Ranaldi, M., and Tarchini, L., 2020, The uplift of the Adriatic flank of the Apennines since the Middle Pleistocene: New insights from the Tronto River basin and the Acquasanta Terme
945 Travertine (central Italy): Geomorphology, 352, https://doi.org/10.1016/j.geomorph.2019.106990.

Snyder, N. P., Whipple, K. X., Tucker, G. E., and Merritts, D. J., 2000, Landscape response to tectonic forcing: Digital elevation model analysis of stream profiles in the Mendocino triple junction region, northern California: Geological Society of America Bulletin, 112,
950 1250-1263.

Tarquini S., Isola I., Favalli M., Battistini A., 2007, TINITALY, a digital elevation model of Italy with a 10 m-cell size (Version 1.0) [Data set]. Istituto Nazionale di Geofisica e Vulcanologia (INGV). https://doi.org/10.13127/TINITALY/1.0.

Thomson, S. N., Brandon, M. T., Reiners, P. W., Zattin, M., Isaacson, P. J., and Balestrieri, M. L.,
955 2010, Thermochronologic evience for orogen-parallel variability in wedge kinematics during extending convergent orogenesis of the northern Apennines, Italy: Geological of America Bulletin, 122, 1160-1179.

Turco, E., Roman, A., Pistolesi, E., Galdenzi, S., Roscioni, M., and Pambianchi, G., 2009, Carta Geologica D'Italia Tolentino Foglio 302, Servizio Geologico D'Italia, ISPRA, scale, 1:50,000.

Twidale, C.R., 1966, Chronology of denudation in the southern Flinders ranges, South Australia: Transactions of the Royal Society of South Australia, v. 90, p. 3–28.

Wegmann, K. W. and Pazzaglia, F. J., 2009, Late Quaternary fluvial terraces of the Romangna and Marche Apennines, Italy: Climatic, lithologic, and tectonic controls on terrace genesis in an active orogen: Quaternary Science Reviews, 28, 137-165, doi:10.1016/j.quascirev.2008.10.006.

Whipple, K. X. and Tucker, G. E., 1999, Dynamics of the stream power river incision model: Implications for height limits of mountain ranges, landscape response timescales and research needs: Journal of Geophysical Research, 104, 17,661–17,674.

Whipple, K.X., 2004, Bedrock rivers and the geomorphology of active orogens: Annual Reviews of Earth Planetary Science, 32, 151-85.

Wilson, L. F., Pazzaglia, F. J., and Anastasio, D. J., 2009, A fluvial record of active fault-propagation folding, Salsomaggiore anticline, northern Apennines, Italy: Journal of Geophysical Research, 114, doi:10.1029/2008JB005984.

Wittmann, H., Malusà, M.G., Resentini, A., Garzanti, E., and Niedermann, S., 2016, The cosmogenic record of mountain erosion transmitted across a foreland basin: Source-to-sink analysis of in situ ^{10}Be, ^{26}Al and ^{21}Ne in sediment of the Po river catchment: Earth and Planetary Science Letters, 452, p. 258–271.

33

FIGURES

990

995

1000

1005
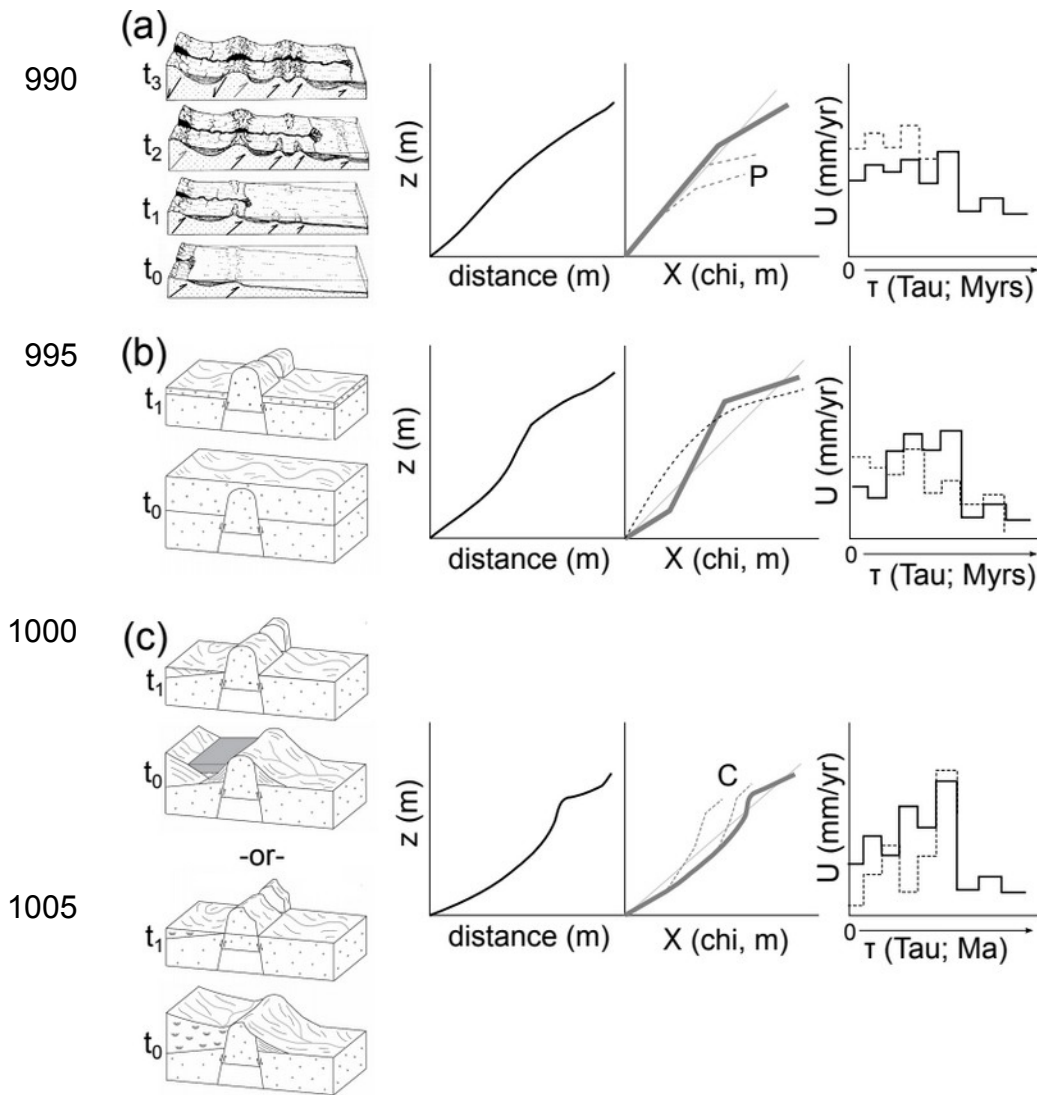
1010 **Figure 1.** Summary of mechanisms of transverse drainages in the context of different base level
fall and drainage area change processes, accompanied by schematic long profile, χ-z and τ-U
plots. (a) Syn-tectonic progressive superposition adapted and modified from Mazzanti and
Trevisan (1978), Alvarez (1999), and Mayer et al., (2003). Black arrows indicate active faults;
gray arrows indicate inactive faults in the block diagram. Loss of headwater drainage,
1015 represented by the convex dashed lines below the main χ-z trend is consistent with stream piracy
(P). The impact of that drainage loss may be predicted in the model as steadily increasing uplift
rates, represented by the dashed line in the τ-U plot. (b) Regional superposition across formerly

34

buried, hard rocks of rivers that developed on a substrate now removed by erosion (modified from Douglass et al., 2009). The χ-z plot is expected to be kinked, resulting in impulsive uplift in the τ-U plot that may be driven by tectonic, dynamic, or both rock uplift processes. Dynamic processes might be in a phase of decay (solid gray line) or growth (dashed lines). (c) Capture (C) of headward streams and growth of catchment area by basin spill-over or asymmetric divide migration processes (modified from Douglass et al., 2009). The χ-z plot is expected to be kinked, but also include a concave segment related to impulsive growth of catchment area. The impact of that growth would be a shallowing of the χ-z plot towards the present and a decrease in the τ-U plot shown by the dashed lines.

1020

1025

1030

1035

1040

1045
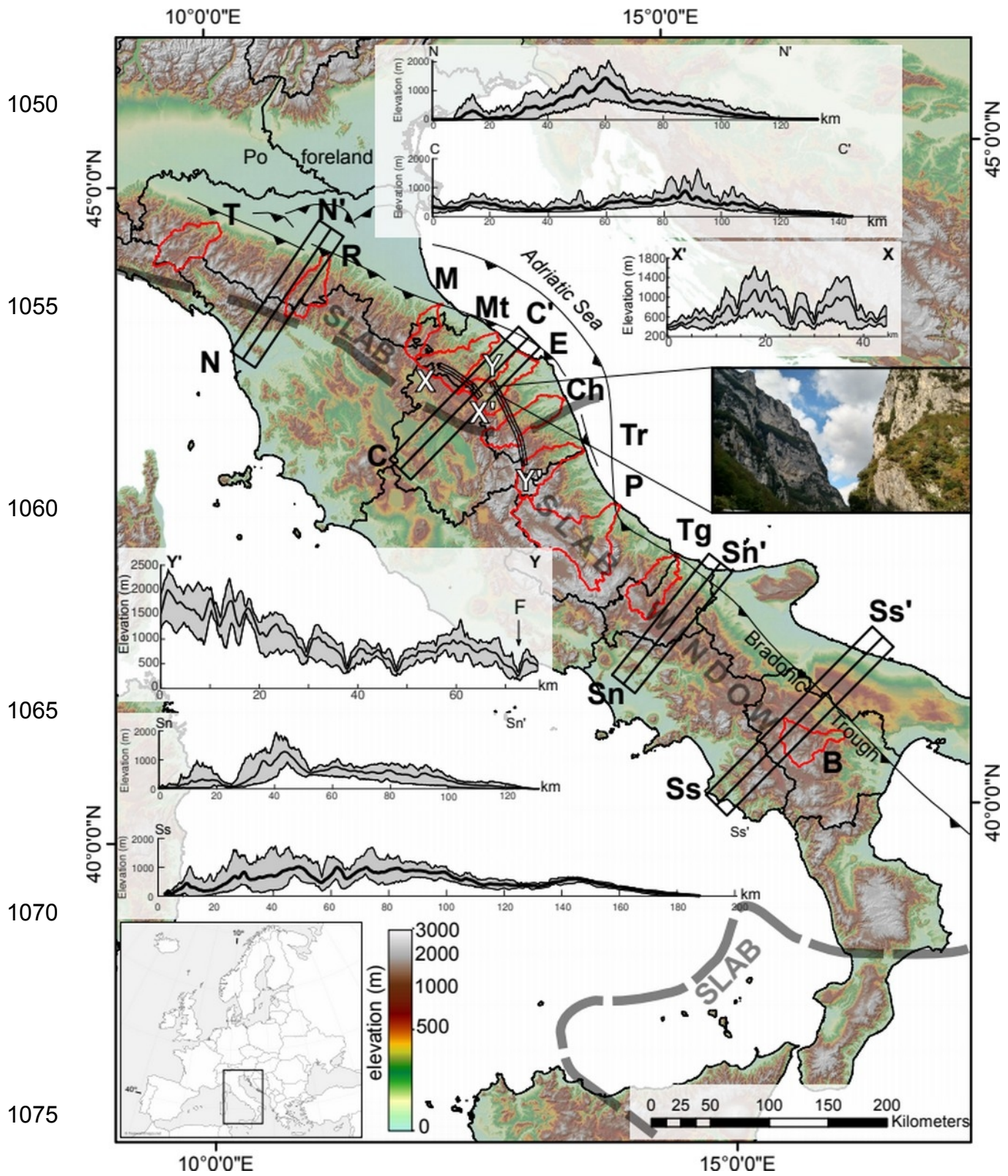
Figure 2. Map of the study area showing the ten catchments in red outline, topographic swath profiles as black boxes, and the relative locations of the intact Adriatic slab and slab window (Faccenna et al., 2014). Catchments, from north to south are Taro (T), Reno (R), Marecchia (M), Metaro (Mt), Esino (E), Chienti (Ch), Tronto (Tr), Pescara (P), Trigno (Tg), and Basento (B). Topographic swath profile X-X' reproduces Fig. 8A of Alvarez (1999). Swath profile Y-Y' stretches along the Marche Ridge from the Sibillini mountains in the south to the Esino River valley in the north. F=Frasassi gorge, an example of a 600 m-deep transverse canyon, shown in the inset photo, carved through massive Mesozoic limestone by the Sentino River.
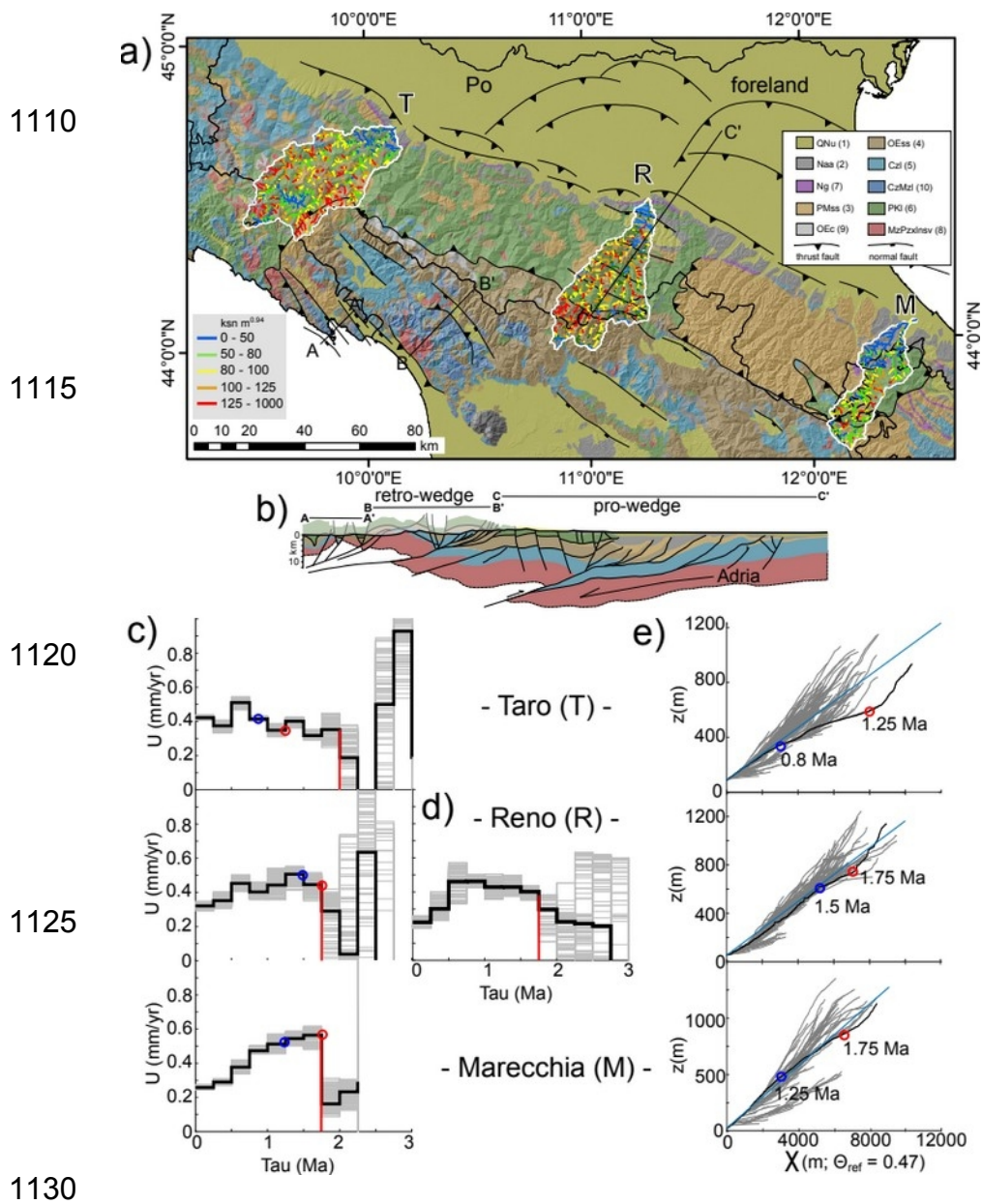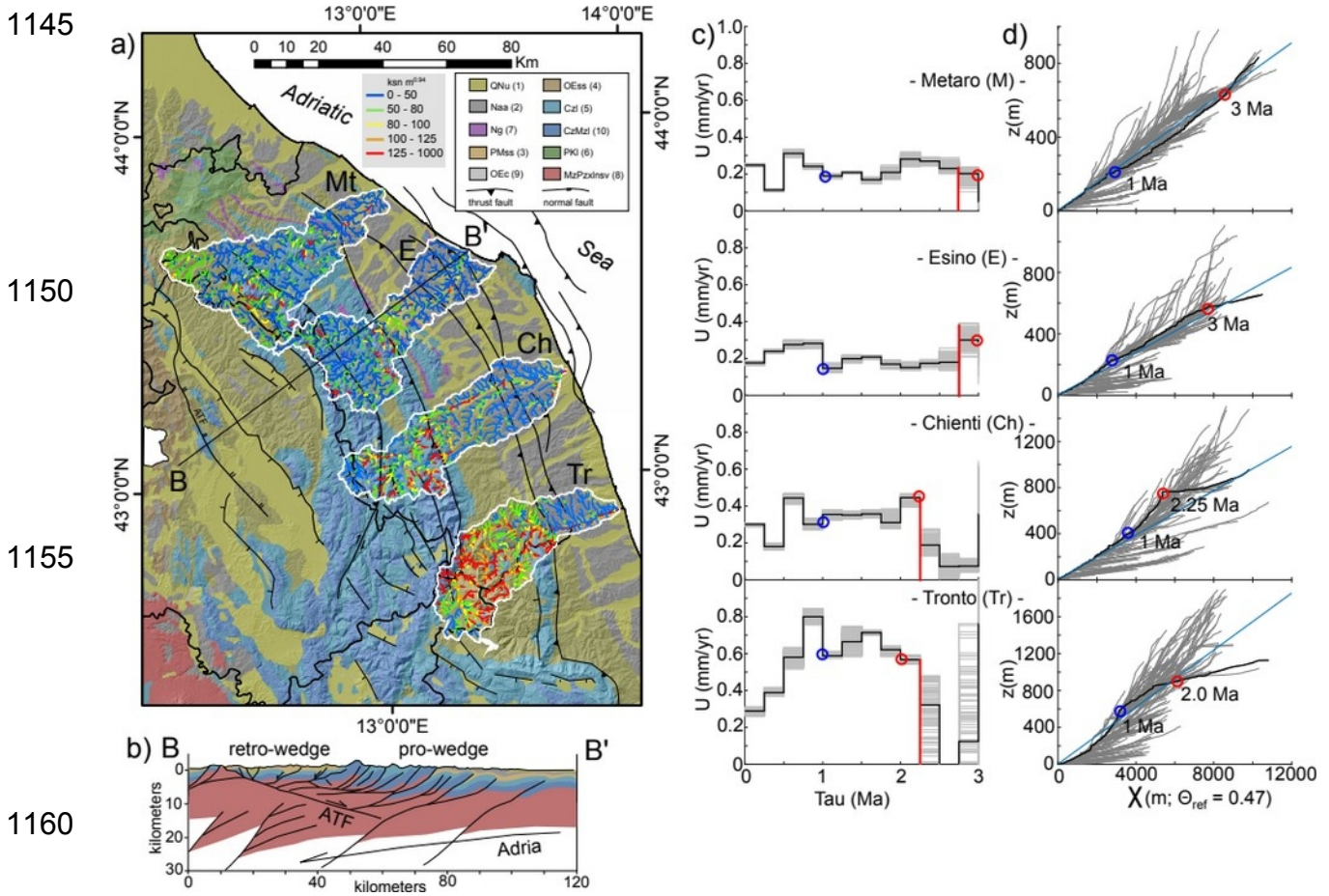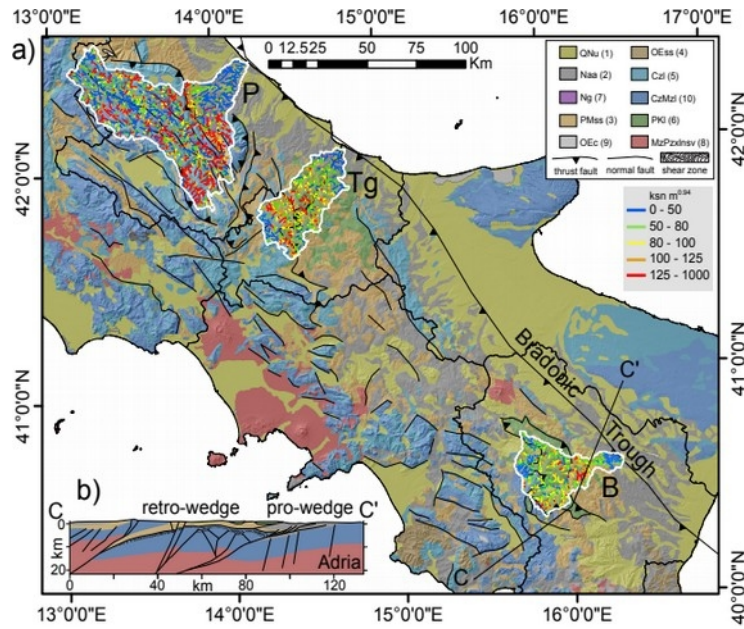
Figure 3. (a) Map of the northern Apennines showing the catchments (white outlines), the distribution of normalized stream steepness (colored channels), and generalized geologic units (see legend and Table 2) and faults summarized from the 1:500,000 geologic map of Italy (http://sgi2.isprambiente.it/arcgis/services/servizi/cartageologica500k/MapServer/WmsServer). Catchment symbols as in Figure 2 and Table 1. (b) Cross section through the northern Apennines (modified from Gunderson et al., 2018). (c) the modeled record of the rate of base level fall as τ-U plots where the thick black line represent the median of 100 monte carlo simulations

represented by the thin gray lines. The vertical red line marks the time when monte carlo simulations have a variation in $U \leq 0.1$ mm/yr. (d) same as (c) for the Reno catchment, except modeled with a uniform, rather than geologic unit variable K. (e) Corresponding $\chi\text{-}z$ plots where the black line indicates the trunk channel, gray lines indicates the tributaries, and the blue line shows the mean trend of all channels. Blue and red circles on the $\chi\text{-}z$ plots are mapped into their corresponding response times in the $\tau\text{-}U$ plots in (c). See S4 for $\tau\text{-}z$ plots.

Figure 4. (a) Map of the central Apennines showing the catchments (white outlines), the distribution of normalized stream steepness (colored channels), and generalized geologic units (see legend and Table 2) and faults summarized from the 1:500,000 geologic map of Italy (http://sgi2.isprambiente.it/arcgis/services/servizi/cartageologica500k/MapServer/WmsServer). Catchment symbols as in Figure 2 and Table 1. ATF = Alto-Tiburina Fault. (b) Cross section
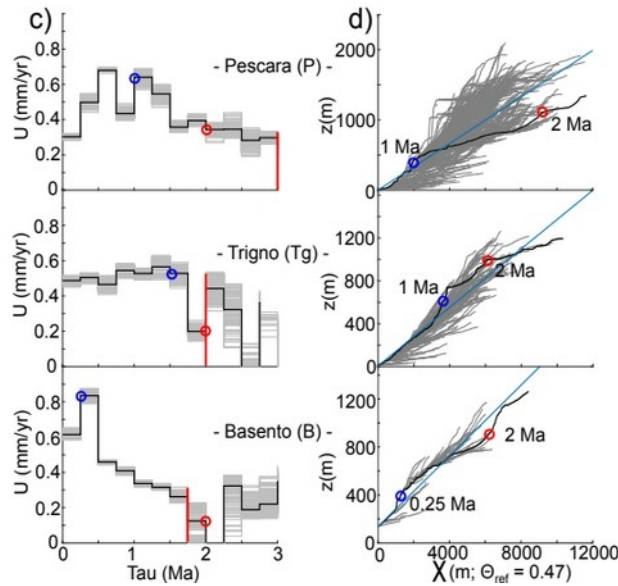
through the central Apennines (modified from Artoni, 2013; Barchi et al., 1999). (c) the modeled record of the rate of base level fall as τ-U plots where the thick black line represent the median of 100 monte carlo simulations represented by the thin gray lines. The vertical red line marks the time when monte carlo simulations have a variation in $U \leq 0.1$ mm/yr. (d) Corresponding χ-z plots where the black line indicates the trunk channel, gray lines indicates the tributaries, and the blue line shows the mean trend of all channels. Blue and red circles on the χ-z plots are mapped into their corresponding response times in the τ-U plots in (c). See S4 for τ-z plots.

40

Figure 5. (a) Map of the southern Apennines showing the catchments (white outlines), the distribution of normalized stream steepness (colored channels), and generalized geologic units (see legend and Table 2) and faults summarized from the 1:500,000 geologic map of Italy (http://sgi2.isprambiente.it/arcgis/services/servizi/cartageologica500k/MapServer/WmsServer). Catchment symbols as in Figure 2 and Table 1. (b) Cross section through the southern Apennines (modified from Mazzoti et al., 2014). (c) the modeled record of the rate of base level fall as τ-U plots where the thick black line represent the median of 100 monte carlo simulations represented by the thin gray lines. The vertical red line marks the time when monte carlo simulations have a variation in U $\leq$ 0.1 mm/yr. (d) Corresponding χ-z plots where the black line indicates the trunk channel, gray lines indicates the tributaries, and the blue line shows the mean trend of all channels. Blue and red circles on the χ-z plots are mapped into their corresponding response times in the τ-U plots in (c). See S4 for τ-z plots.
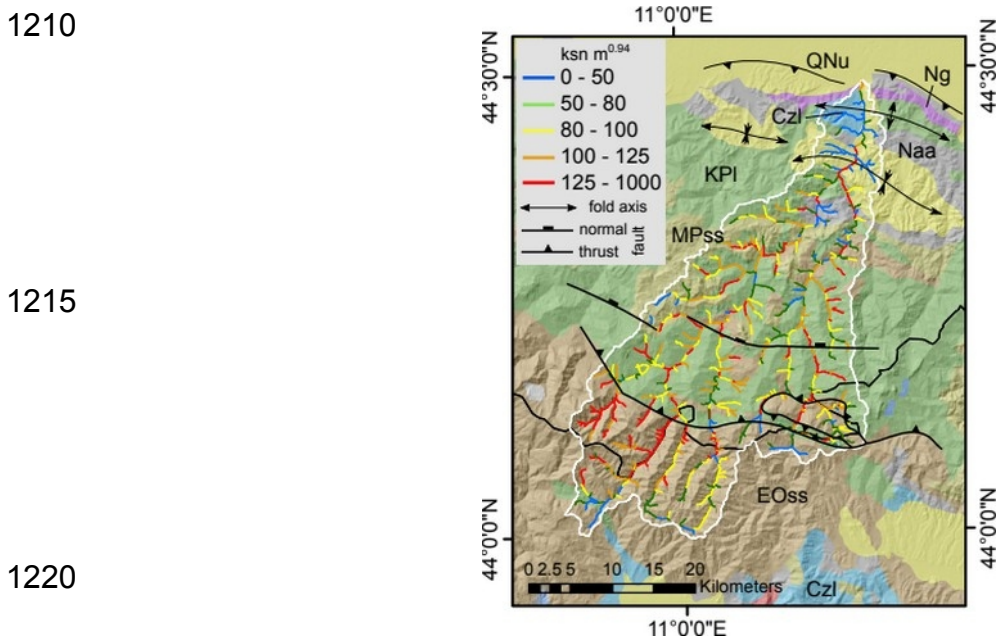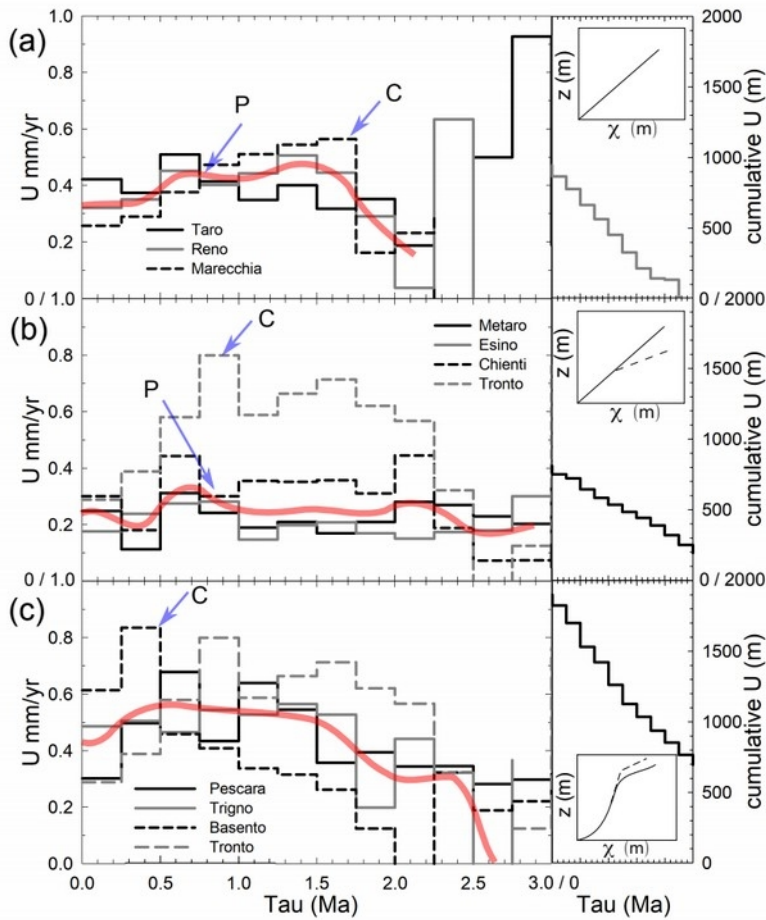

Figure 6. Geologic map of the Reno catchment showing the distribution of normalized channel steepness (k_{sn}), rock-type, and major geologic structures traversed by the Reno River. Geologic unit symbols are in Table 2.

Figure 7. Combined median τ-U plots for the (a) northern Apennine, (b) central Apennine, and (c) southern Apennine catchments, with accompanied representative χ-z plots and the cumulative uplift curves for a representative catchment for the past 3 Ma. Transparent red line is the respective mean τ-U. This mean does not include the Tronto catchment in (b). P = possible examples of stream piracy and loss of drainage area; C = possible examples of stream capture and growth of drainage area.

Supplementary Information

S1. ^{10}Be TCN concentrations and Cronus calculator model of erosion rates for the Basento
1260   catchment.

S2. Excel data sheet of the weighted mean erodibility values and uncertainties, stream steepness,
and erosion rate data.

S3. Tau-z plots for the ten analyzed catchments. Color bar is scaled to the different rock types in
Table 2.

1265   S4. MatLab scripts and sample input catchment and geology text files for the Reno catchment.